Electronic, dielectric, and optical properties of photonic crystals composed of TiO$_2$ nanoparticles three-dimensional arrays: the first principles calculations

Ruslana Balabai
Dariya Kravtsova
Pavlo Merzlykin
Yuliya Prihozhaya

Electronic, dielectric, and optical properties of photonic crystals composed of TiO₂ nanoparticles three-dimensional arrays: the first principles calculations

Ruslana Balabai, Dariya Kravtsova,* Pavlo Merzlykin, and Yuliya Prihozhaya
Kryvyi Rih State Pedagogical University, Kryvyi Rih, Ukraine

Abstract. Opal photonic crystals (PCs), composed of TiO₂ nanoparticles, three-dimensional array were simulated. This paper shows how electronic, dielectric, and optical properties of such PCs depend on the shape of structural elements, their polymorphic modifications, and the parameters of their stacking in the body's space of metastructure. © *2018 Society of Photo-Optical Instrumentation Engineers (SPIE)* [DOI: 10.1117/1.JNP.12.036003]

1 Introduction

Photonic crystals (PCs) consist of periodically located particles of materials (submaterials) with different refractive indices. Periodic spatial modulations of the refractive index create regions called photonic band gaps or stop zones. Therefore, the PCs reflect incident light at certain frequencies and angles, depending on the spatial location of submaterials along one or more principal axes of one-, two-, and three-dimensional (3-D) periodic structures.[1] The width of the photonic band gap is determined by the contrast between the refractive index of the submaterials, the parameters of structural symmetry and the lattice. PC's color is a consequence of their micro- and nanostructures that selectively reflect a certain range of wavelengths of incident light. This mechanism is the basis of structural colors, which are abundant in nature: in plants, insects, and mollusks.[2]

Influence on the PC or the chemical composition, the shape, the crystalline structure of the forming elements, or regulation of the parameters of their stacking in the PCs allows to control not only electronic properties but also photonic band gap. Thus, the look of the PC can be modified in a controlled manner.[1] The electrically sensitive PCs represent one of the most promising controlled metamaterials for technological applications. In fact, the electrical effects can be accurately regulated and continuously controlled. In addition, their implementation is convenient and usually characterized by a quick reaction response.[3,4] For example, McPhail et al.[5] created electrically regulated 3-D PCs, which can adjust the wavelengths in the range of 70 nm. The supply of a voltage perpendicularly to the layers of the PC led to reorganization of its components and, thus, to change in the index of refraction of the entire structure. It is a mechanism of the influence on the photonic band gap directly.

Zhang et al.[6] announce the creation of the ordered array of TiO₂ nanotubes (Fig. 1) in anatase modification and a mixture of rutile and anatase phases. They describe the origin of nanotubes' structural anisotropy and measure anisotropic dielectric permittivity of the experimental samples.

---

*Address all correspondence to: Dariya Kravtsova, E-mail: gritsulia.dariya@kdpu.edu.ua
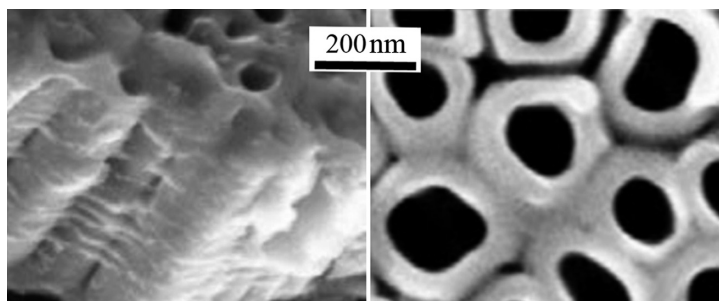
Fig. 1 The images of an experimental sample of TiO_2 nanotubes array taken with an electron microscope.[6]

This paper shows how electronic and dielectric properties of such PCs depend on the shape of structural elements, their polymorphic modifications, and the parameters of their stacking in the body's space of metastructure.

Traditionally, the analysis of optical, dielectric, and photonic properties is done by the theoretical and calculation methods, for example, Refs. 7–9. Hybertsen and Louie[10] propose to determine the dielectric properties by the density functional theory methods. Therefore, this result is performed using the software package.[11] The used software is the unique author's code, which has several advantages. First, the authors take responsibility for any errors of algorithmic or mathematical nature in their own product. Second, the software has been successfully tested in many of the author's scientific papers.[12–16] Third, the process of scientific physical analysis of the calculation result is more flexible if you have your own open source. It makes possible the analyzing of the results of any intermediate stage and viewing any data—not only programmed by the third party developer. In addition, the independent improvement of software according to specific needs of the research is also convenient. Due to the fact that the software package is not yet registered, Ref. 11 contains a tool for control calculation of the total energy of the silicon crystal, the spatial distribution of density, and density of states of the valence electrons.

2 Methods

The basic states of the electron–nucleus systems were detected by means of the self-consistent solution of the Kohn–Sham equations. Electronic variables were determined only with the atomic cores fixed. Following Kohn–Sham,[17,18] electronic density was written down in terms of occupied orthonormal one-particle wave functions:

$$n(\mathbf{r}) = \sum_i |\psi_i(\mathbf{r})|^2. \qquad (1)$$

The point on the potential energy surface in the Born–Oppenheimer approximation was determined as a minimum energy functional with regard to the wave functions:

$$E[\{\psi_i\}, \{R_j\}, \{\alpha_\nu\}] = \sum_i \int_\Omega d^3 r \psi_i^*(\mathbf{r}) \left[-\frac{\hbar^2}{2m} \nabla^2 \right] \psi_i(\mathbf{r}) + U[\{n(\mathbf{r})\}, \{R_j\}, \{\alpha_\nu\}], \qquad (2)$$

where $\{R_j\}$ are coordinates of atomic cores and $\{\alpha_\nu\}$ are any external influences on the system.

In the generally accepted formulation, minimization of the energy functional [Eq. (2)] with respect to one-particle orbitals with additional orthonormal constraint on the one-particle orbitals $\psi_i(\vec{r})$ results in Kohn–Sham one-particle equations:[18]

$$\left\{ -\frac{\hbar^2}{2m} \nabla^2 + \frac{\partial U}{\partial n(\mathbf{r})} \right\} \psi_i(\mathbf{r}) = \varepsilon_i \psi_i(\mathbf{r}). \qquad (3)$$

In the solution of these equations, the pseudopotential formalism was used, according to which a solid is considered as a set of valence electrons and the ion cores. In the pseudopotential

approximation, the operator of the pseudopotential V_{PS}, which describes the interaction of valence electrons with the core, is small, and the corresponding pseudo-wavefunction is smooth. Pseudopotential is required to correctly represent the long-range interactions of the core and to produce pseudo-wavefunction solutions that approach the full wavefunction outside a core radius r_c. In addition, it is desired for a pseudopotential to be transferable, which means that one and the same pseudopotential can be used in calculations of different chemical environment resulting in calculations with comparable accuracy. For example, Bachelet et al.[19] proposed an analytic fit to the pseudopotentials. This ab initio pseudopotential is used by us.

The full crystalline potential is constructed as the sum of ion pseudopotentials that are not overlapping and associated with ions (nucleus + core electrons), located at the $\mathbf{R}_S$ positions that are periodically repeated for crystals:

$$V_{\text{cryst}}(\mathbf{r}) \rightarrow V_{PS}(\mathbf{r}) = \sum_{\mathbf{p}} \sum_{S} \hat{V}_S^{PS}(\mathbf{r} - \mathbf{p} - \mathbf{R}_S). \tag{4}$$

For nonperiodic systems, such as a thin film or a cluster, the problem of lack of periodicity is circumvented by using of the supercell method.[20,21] Namely, the cluster is periodically repeated but the distance between each cluster and its periodic images is so large that their interaction is negligible. The ubiquitous periodicity of the crystal (or artificial) lattice produces a periodic potential and thus imposes the same periodicity on the density (implying Bloch's theorem). The Kohn–Sham potential of a periodic system exhibits the same periodicity as the direct lattice and the Kohn–Sham orbitals can be written in Bloch form:

$$\psi(\mathbf{r}) = \psi_i(\mathbf{r}, \mathbf{k}) = \exp(i\mathbf{k} \cdot \mathbf{r})u_i(\mathbf{r}, \mathbf{k}), \tag{5}$$

where $\mathbf{k}$ is a vector in the first Brillouin zone. The functions $u_i(\mathbf{r}, \mathbf{k})$ have the periodicity of the direct lattice. The index i runs over all states. The periodic functions $u_i(\mathbf{r}, \mathbf{k})$ are expanded in the plane wave basis. This heavily suggests using plane waves as the generic basis set in order to expand the periodic part of the orbitals. Since plane waves form a complete and orthonormal set of functions, they can be used to expand orbitals according to

$$\Psi_j(\mathbf{k}, \mathbf{r}) = \frac{1}{\sqrt{N_0}\sqrt{\Omega}} \sum_{\mathbf{G}} b_J(\mathbf{k} + \mathbf{G}) \exp[i(\mathbf{k} + \mathbf{G})\mathbf{r}], \tag{6}$$

where $\mathbf{G}$ is the vector in the reciprocal space, Ω is the volume of the elementary cells, which consists of a periodic crystal or an artificial superlattice when reproducing nonperiodic objects.

Equation (3) after the Fourier transform to the reciprocal space has the form:

$$\sum_{\mathbf{G}} \left[\left\{ \frac{\hbar^2}{2m}(\mathbf{k} + \mathbf{G})^2 - \varepsilon_j \right\} \delta_{\mathbf{G},\mathbf{G}'} + V_{KS}(\mathbf{k} + \mathbf{G}, \mathbf{k} + \mathbf{G}') \right] b_j(\mathbf{k} + \mathbf{G}) = 0, \tag{7}$$

where V_{KS} is the Kohn–Sham potential:

$$V_{KS}(\mathbf{k} + \mathbf{G}, \mathbf{k} + \mathbf{G}') = V_{ps}(\mathbf{k} + \mathbf{G}, \mathbf{k} + \mathbf{G}') + V_H(\mathbf{G}' - \mathbf{G}) + V_{XC}(\mathbf{G}' - \mathbf{G}), \tag{8}$$

where V_{xc} is the exchange and correlation potential. To calculate it, we used Ceperley–Alder's approximation that has been parameterized by Perdew and Zunger.

In the general case, the expressions describing the potentials of interactions are complex. The use of the atomic bases containing the inversion operation in the point symmetry group leads to the fact that the Fourier components in the expansion of all expressions are real.

The main value in the formalism of the functional of the electron density is the charge density. It is estimated from a self-consistent solution of Eq. (7), which should be performed at all points of the nonreduced section of the Brillouin zone:

$$n(\mathbf{G}) = \frac{2}{N_T} \sum_{\mathbf{k}} \sum_{j} \sum_{\alpha \in T} \sum_{\mathbf{G}'} b_j^*(\mathbf{k} + \mathbf{G}' + \alpha\mathbf{G})b_j(\mathbf{k} + \mathbf{G}'), \tag{9}$$

where the index j runs over all occupied states, $\mathbf{k}$ is a vector in the first Brillouin zone, N_T is the number of the operators α in the point group T of the atomic basis, and the factor 2 takes into account the spin degeneracy.

Estimated effort can be reduced if there is the integral over the Brillouin zone to approximate by summing over special points of the Brillouin zone. It is possible to replace (with satisfactory precision) the summation by the finite number of special points to one point in the Brillouin zone. It is possible to restrict only the Γ-point in the Brillouin zone, especially as it relates to the artificial periodic systems.

Distribution of electrons along the energy zones for Γ-state of the investigated structures was found by means of numerical calculation of derivative $\lim_{\Delta E \to 0} \Delta N / \Delta E$ (where ΔN is a number of the allowed states for the ΔE interval of energy). The one-particle energy spectrum was obtained from the calculation of the eigenvalues of the Kohn–Sham matrix. In accordance with ideology of the electronic density functional, the occupied states at absolute zero temperature were defined. It allowed to define position of the last occupied state, their number being half the number of electrons (due to ignoring the spin of the electron), and position of the first free states.

The solid-state linear response to perturbation is described by a dielectric matrix. In our computational experiments, the static dielectric matrix was estimated from the electronic structure of the ground state of the crystalline system (occupied and unoccupied states). The dielectric matrix $\epsilon_{\mathbf{GG}'}^{-1}(\mathbf{q}, \omega)$ was calculated in reciprocal space and depended on the wave vector $\mathbf{q}$ and the oscillation frequency of electromagnetic field ω ($\mathbf{G}$, reciprocal lattice vectors). Nondiagonal elements of the matrix $\epsilon_{\mathbf{GG}'}^{-1}$ determine the local effects of the field. The macroscopic dielectric function was as follows:[10]

$$\epsilon_M(\mathbf{q} + \mathbf{G}) = \frac{1}{\epsilon_{00}^{-1}(\mathbf{q})}. \tag{10}$$

To get the elements of the matrix, the equation in the reciprocal space was solved:

$$\epsilon_{\mathbf{GG}'}^{-1}(\mathbf{q}) = \delta_{\mathbf{GG}'} + \frac{4\pi e^2}{|\mathbf{q} + \mathbf{G}|^2} \chi_{\mathbf{GG}'}(\mathbf{q}), \tag{11}$$

where polarization was defined as follows:

$$\chi_{\mathbf{GG}'}(\mathbf{q}) = \sum_{\mathbf{G}''} A_{\mathbf{GG}''}^{-1}(\mathbf{q}) \chi_{\mathbf{G}''\mathbf{G}'}^0(\mathbf{q}), \tag{12}$$

$$A_{\mathbf{GG}'}(\mathbf{q}) = \delta_{\mathbf{GG}'} - \chi_{\mathbf{GG}'}^0(\mathbf{q}) \frac{4\pi e^2}{|\mathbf{q} + \mathbf{G}|^2} - \sum_{\mathbf{G}''} \chi_{\mathbf{GG}'}^0(\mathbf{q}) K_{xc}(\mathbf{G}'' - \mathbf{G}'), \tag{13}$$

$$\chi_{\mathbf{GG}'}^0(\mathbf{q}) = \frac{4}{\Omega} \sum_{c,v,\mathbf{k}} \frac{\langle v, \mathbf{k} | e^{-i(\mathbf{q}+\mathbf{G})\mathbf{r}} | c, \mathbf{k} + \mathbf{q} \rangle \langle c, \mathbf{k} + \mathbf{q} | e^{i(\mathbf{q}+\mathbf{G}')\mathbf{r}'} | v, \mathbf{k} \rangle}{\varepsilon_{v,\mathbf{k}} - \varepsilon_{c,\mathbf{k}+\mathbf{q}}}, \tag{14}$$

where the indices c, v, $\mathbf{k}$ are taken over by the states of conduction, valence, and Brillouin zones, respectively.[10]

The resulting dielectric matrix is Hermitian and, due to the presence of the center of inversion of the model crystal, is symmetric. Its diagonalization leads to the obtaining of eigenvalues $\epsilon_n^{-1}(\mathbf{q})$ and eigenfunctions $V_n^{-1}(\mathbf{q} + \mathbf{G})$:

$$\sum_{\mathbf{G}'} \epsilon^{-1}(\mathbf{q} + \mathbf{G}, \mathbf{q} + \mathbf{G}') V_n^{-1}(\mathbf{q} + \mathbf{G}') = \varepsilon_n(\mathbf{q}) V_n^{-1}(\mathbf{q} + \mathbf{G}). \tag{15}$$

They serve to visualize screening in real space, transmit information about the solid-state electronic response and allow taking into account the symmetry of the crystal adequately. Eigenvalues mean the dielectric band structure. As in Refs. 22 and 23, we interpret the obtained

eigenvalues of the dielectric matrix as the absorption spectrum. The positions of the optical transitions are determined from the ground-state band structure (Kohn–Sham eigenvalues) by applying the optical selection rules.

3 Result and Discussion

To continue the investigation of arrayed TiO_2 nanoparticles photonic properties, we theoretically analyzed the changes in the electrochemical, dielectric, dispersive properties of the opal-type PCs depending on the shape of TiO_2 structural elements, and parameters of their stacking inside the crystal body. Computer numerical models for quantitative evaluation of the characteristics of the PCs made of TiO_2 rutile nanoparticles of various shapes (nanospheres, nanotubes, nanocylinders, ellipsoids), stacked into the spatial structure of tetragonal symmetry, have been developed. The nanosphere [Fig. 2(a)] was a cluster of 33 atoms (11 — Ti, 22 — O), the nanotube [Fig. 2(b)] contained 48 atoms (16 — Ti, 32 — O), the nanocylinder [Fig. 2(c)] contained 57 atoms (19 — Ti, 38 — O), and the nanoelipsoid [Fig. 2(d)] contained 16 atoms (6 — Ti, 10 — O). The diameter of the nanospheres, nanotubes, and nanocylinders was 7.4 Å. The short diameter of the ellipsoid was 4.6 Å, the long diameter of the ellipsoid was 5.9 Å, and the height of the nanotube and the cylinder was 8.9 Å.

The arranging of the tetragonally symmetric PC forming elements occurred with a constant c parameter, equal to 9.52 Å and variables a and b parameters of the crystal spatial lattice, ranged between 4.76 and 11.64 Å. Such a variation of spatial ordering of the forming elements influenced the electronic and dielectric properties of the obtained PC. Therefore, depending on the period of forming elements' arranging in the plane of the vectors **a** and **b**, the electronic and dielectric properties of the PCs were determined and by means of a comparative analysis, the anisotropy of their properties was determined.

The forming elements of the modeled cubically symmetric PC consisted of rutile and anatase TiO_2 nanoparticles. The nanoparticles were the clusters of 18 atoms (6 — Ti, 10 — O). The rutile nanoparticle size was $6.4 \times 4.6 \times 5.9$ Å [Fig. 3(a)], and the anatase one was $3.8 \times 3.2 \times 5.7$ Å
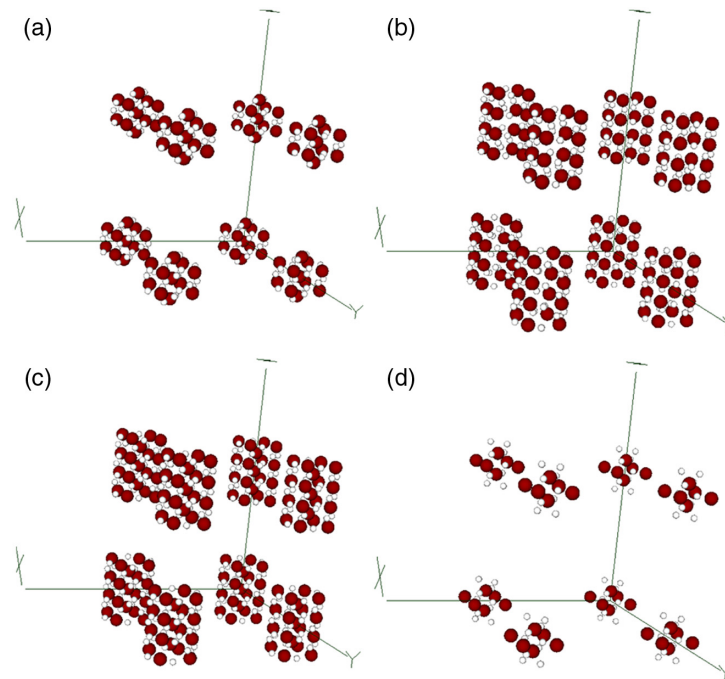
Fig. 2 Atomic models of the tetragonally symmetric rutile TiO_2 modification PCs: an array of (a) nanospheres, (b) nanotubes, (c) nanocylinders, and (d) nanoelipsoids (dark spheres represent Ti atoms and white ones represent O).

(a)   (b)
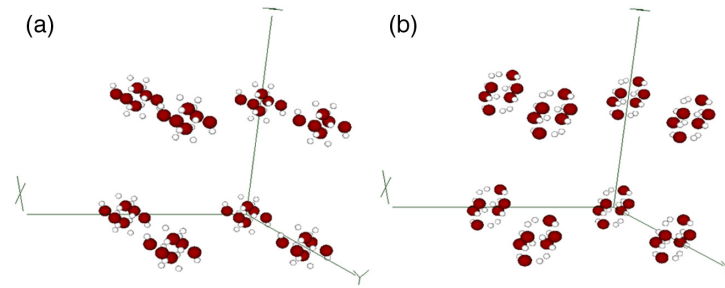
Fig. 3 Atomic models of the cubically symmetric rutile and anatase TiO$_2$ PCs: (a) an array of rutile nanoparticles and (b) an array of anatase nanoparticles (dark balls represent Ti atoms, white ones represent O).

[Fig. 3(b)]. The arranging period varied across all three vectors with a step of 0.53 Å from 6.35 to 10.05 Å.

Figure 4 shows the graphs of band gap width change of the tetragonally symmetric 3-D PCs, depending on the period of forming elements' arranging along the directions a and b. Regardless of the shape of the crystals' structural elements, peaks occur in periods of 8 to 10 Å. Therefore, we can assume that the properties of the PC made up of nanoparticles up to 10 Å do not depend on the shape of the nanoparticle, but only from the period of their repetition in the metastructure's body.

Figure 5 shows the graphs of the atomic systems' total energy dependence on the period of forming elements' arranging in the tetragonally symmetric PC. The PC, composed of ellipsoidal nanoclusters, shows the smallest values of the atomic system's total energy in the entire range of arranging periods, which indicates a high probability of metastructure, composed of such nanoparticles, compared with other simulated ones. Therefore, for the comparative analysis of the optical properties' anisotropy detection, macroscopic relative permittivity for ellipsoidal TiO$_2$ clusters PC, with the periods of forming elements' arranging along directions a and b equal to 7.9, 9.0, and 10.6 Å, was calculated.

In Table 1, the calculated macroscopic relative permittivities of 3-D PCs in the direction of the electric vector of the external field (E-vector) $\mathbf{E}||Z$, $\mathbf{E} \perp Z$, and $(\mathbf{E}\hat{Z}) \approx 53$ deg are given. It can be seen that the anisotropy of macroscopic permittivity is revealed only in the calculation of PC with the period of forming elements' arranging equal to 7.9 Å.

The tetragonally symmetric PC, composed of nanoellipsoids with a period of 7.9 Å, has a band gap of 2.65 eV/atom, which is close to the band gap value of the TiO$_2$ rutile crystal. Figure 6 shows the band gap width of the cubically symmetric PC, composed of TiO$_2$ rutile and anatase nanoparticles depending on the period of forming elements' arranging. For the calculation of dielectric matrices, the periods of forming elements' arranging were 7.4 and 7.9 Å.
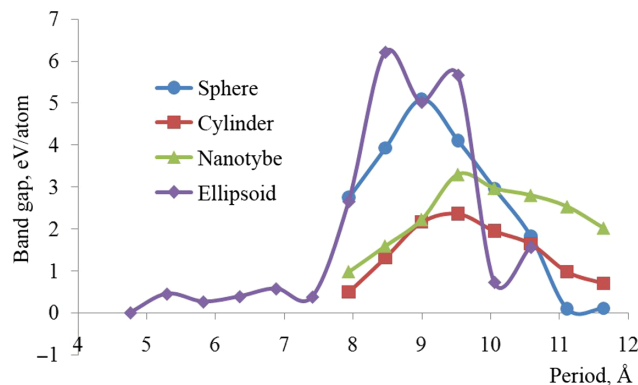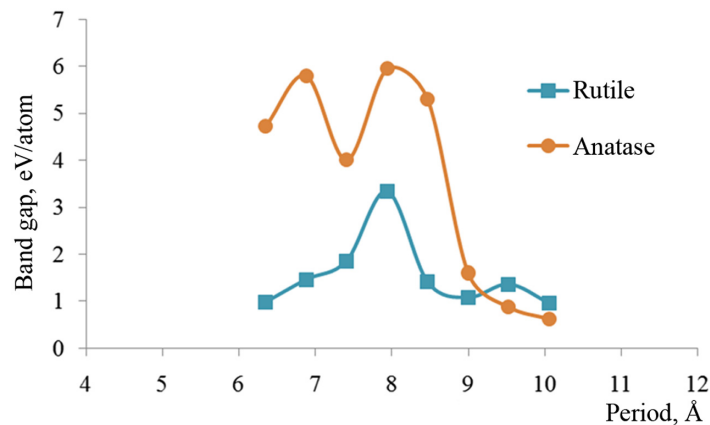

Fig. 4 The width of the band gap as a function of the period ($a = b$) of the spatial tetragonal structure of the PC composed of TiO$_2$ rutile nanoparticles (calculated at the Γ-point of the Brillouin zone).
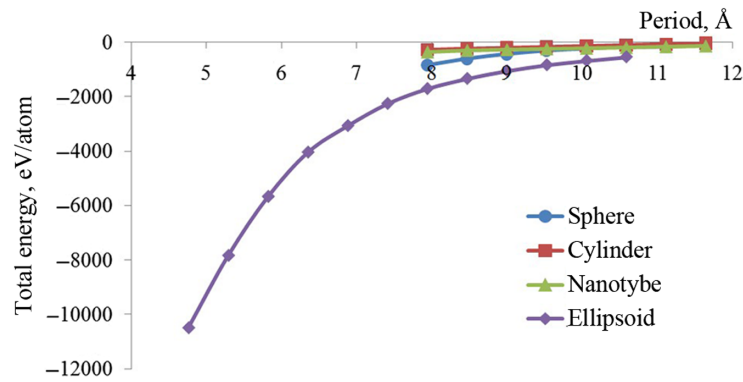
Fig. 5 Total energy as a function of the period ($a = b$) of forming elements' arranging of TiO$_2$ rutile nanoparticles PC with spatial tetragonal structure.

Table 1 Macroscopic relative permittivity of the tetragonally symmetric PCs composed of ellipsoidal TiO$_2$ rutile nanoparticles.
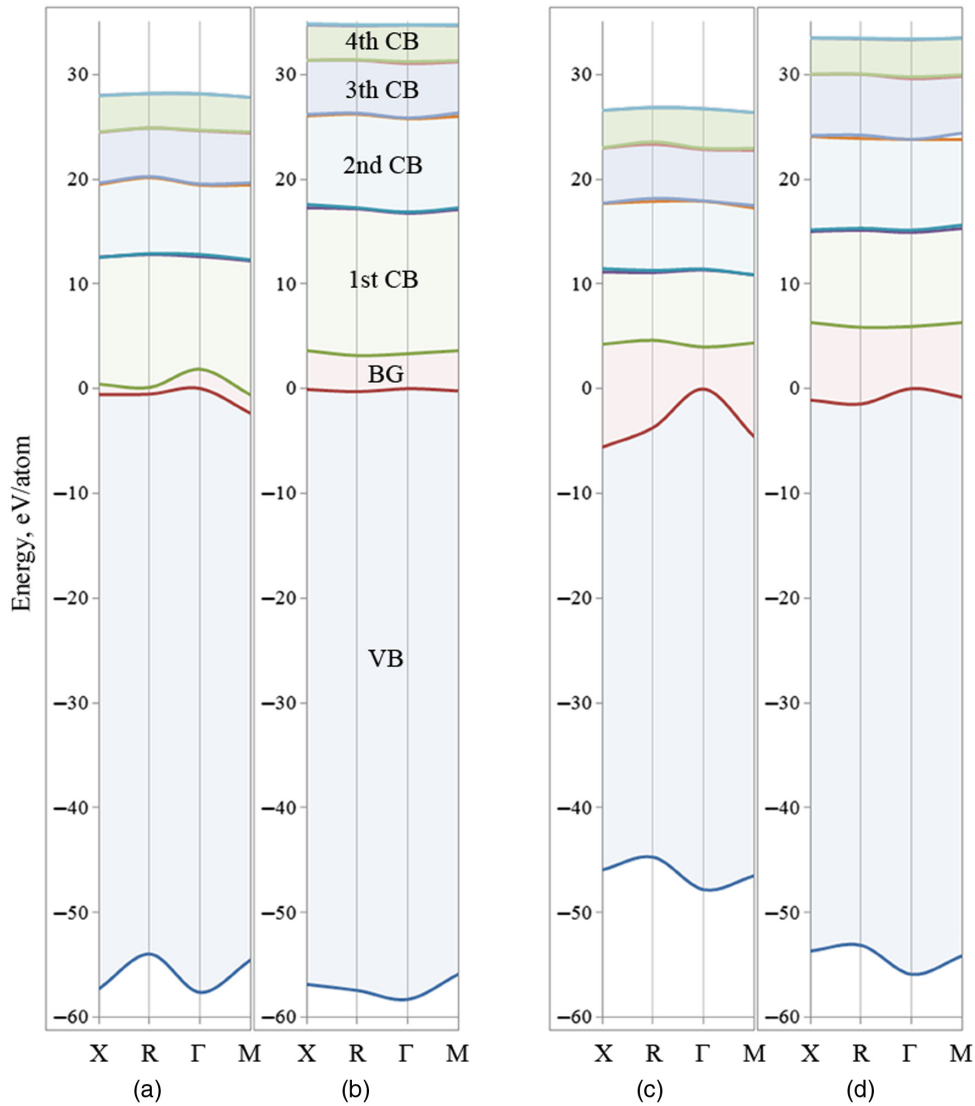
	Period (Å)		
E-vector direction	7,9	9,0	10,6
E‖Z	0,96	0,99	0,99
E ⊥ Z	1,00	0,99	0,99
$(\mathbf{E}\hat{Z}) \approx 53$ deg	1,00	0,99	—

Fig. 6 The band gap width as a function of the period of forming elements' arranging of the cubically symmetric PCs composed of TiO2 rutile and anatase nanoparticles (calculated at the Γ-point of the Brillouin zone).

In Fig. 7, electronic band structures of the cubically symmetric PCs, composed of arranged rutile and anatase nanoclusters with periods of 7.4 and 7.9 Å, are presented. They clearly illustrate that the band structure varies considerably according to the change of period. Considerable changes occurred in the band gap of PC, composed of rutile nanoparticles with the period of forming elements' arranging 7.4 Å. It is atypically narrow for the TiO$_2$ of rutile modification, but with increasing the period to 7.9 Å PC turns into a direct- and wide-gap crystal. This indicates the existence of quantum transitions between the forming elements' crystal, when they are arranged with certain distances.

Fig. 7 The band structures of the cubically symmetric PCs, composed of (a,b) TiO_2 rutile and (c, d) anatase nanoparticles with the periods (a, c) 7.4 Å and (b, d) 7.9 Å.

Table 2 Macroscopic relative permittivity of cubically symmetric PCs composed of TiO_2 nanoparticles of rutile or anatase modifications.

	Rutile		Anatase	
	Period (Å)		Period (Å)	
E-vector direction	7, 4	7, 9	7, 4	7, 9
E∥Z	1,13	1,00	0,99	0,99
E ⊥ Z	0,99	1,00	0,99	1,00

Table 2 shows the macroscopic permittivity of the cubically symmetric PCs, composed of the TiO_2 nanotubes of the rutile and anatase modifications, respectively. It can be seen that the dielectric properties of the PCs, composed of rutile nanoparticles, are anisotropic at the period of forming elements' arranging equaling 7.4 Å. After increasing the period to 7.9 Å, the anisotropy of the macroscopic relative permittivity disappears. The dielectric properties of anatase nanoparticles PCs occur isotropic at these periods.
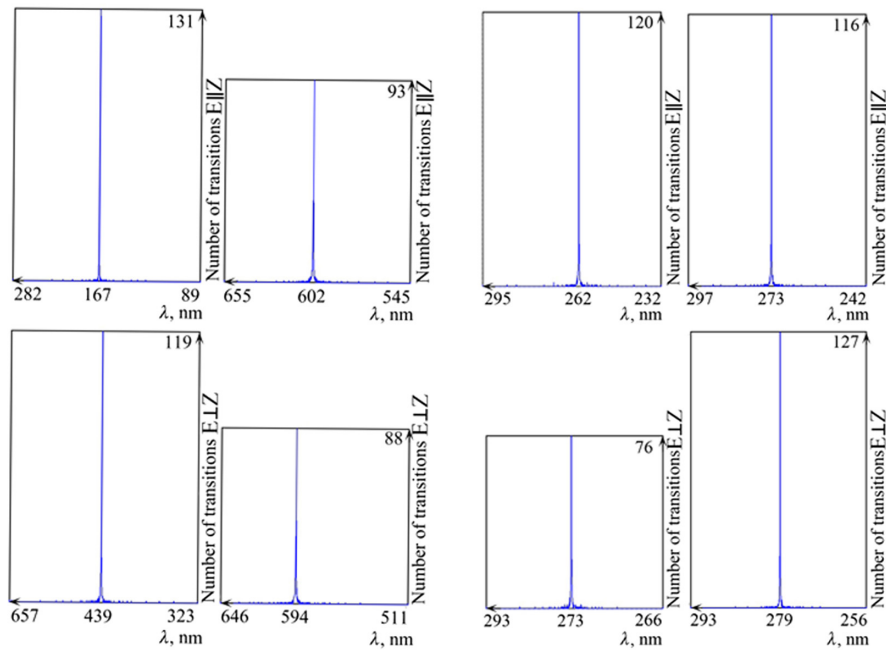
Fig. 8 The dielectric matrices' eigenvalues (absorption spectrums) of the cubically symmetric PCs composed of (a) rutile and (b) anatase TiO$_2$ nanoparticles with the periods of forming elements' arranging (left) 7.4 Å and (right) 7.9 Å.

The optical absorption spectrum is obtained as a solution of Eq. (15) for $q \rightarrow 0$. Here, the vector q denotes the transverse polarization of the electric field E. Thus, Fig. 8 shows the dielectric matrices' eigenvalues of the cubically symmetric PCs of the rutile and anatase modifications with the periods of forming elements' arranging 7.4 and 7.9 Å in the direction of E-vector $E\|Z$ and $E \perp Z$. In PC, composed by arranged rutile nanoparticles with the period of 7.4 Å, the absorption wavelength varies considerably according to the direction of E-vector. When $E\|Z$, a peak in the absorption spectrum is observed at 167 nm, and when $E \perp Z$, at 439 nm. As when comparing of macroscopic relative permittivities, PC's properties occur isotropical with the period of forming elements' arranging 7.9 Å; the peak in the absorption spectrum is in the visible region of ~600 nm.

The anatase nanoparticles PC do not fundamentally change the absorption wavelength with changing the direction of E-vector, and it remains constant when changing the period of forming elements' arranging from 7.4 to 7.9 Å. For any of the calculated models, the wavelength is ~270 nm; thus, PC's properties are isotropic.

4 Conclusion

It was discovered that the electronic and dielectric properties of tetragonally symmetric PCs do not depend on the shape of the nanoparticle, but only from the period of their repetition in the metastructure's body, and in some models, from the direction of E-vector. The anisotropy of dielectric properties was observed in the cubically symmetric PC, composed of rutile nanoparticles with the period of forming elements' arranging equaling 7.4 Å. If the nanoparticles period increased to 7.9 Å and then the anisotropy disappeared. The dielectric properties of anatase nanoparticles PCs were isotropic.

Acknowledgments

References

1. K. Sumioka, H. Kayashima, and T. Tsutsui, "Tuning the optical properties of inverse opal photonic crystals by deformation," *Adv. Mater.* **14**(18), 1284–1286 (2002).
2. F. Di Stasio et al., "Tuning optical properties of opal photonic crystals by structural defects engineering," *J. Eur. Opt. Soc. Rapid Publ.* **4**, 09033 (2009).
3. L. Nucara, G. Francesco, and M. Virgilio, "Electrically responsive photonic crystals: a review," *J. Mater. Chem. C* **3**(33), 8449–8467 (2015).
4. J. Ge et al., "Rewritable photonic paper with hygroscopic salt solution as ink," *Adv. Mater.* **21**(42), 4259–4264 (2009).
5. D. McPhail, M. Straub, and M. Gu, "Electrical tuning of three-dimensional photonic crystals using polymer dispersed liquid crystals," *Appl. Phys. Lett.* **86**(5), 051103 (2005).
6. Y. Zhang et al., "Optical anisotropy in vertically oriented TiO_2 nanotube arrays," *Nanotechnology* **28**(37), 374001 (2017).
7. J. B. Pendry, "Calculating photonic band structure," *J. Phys. Condens. Matter* **8**(9), 1085–1108 (1996).
8. E. Y. Glushko, "Analytical solution for the field in photonic structures containing cubic nonlinearity," *Opt. Commun.* **259**(1), 342–349 (2006).
9. S. I. Pokutnyi and P. P. Gorbyk, "Absorption of light in positron and electron states in quasi-zero–dimensional nanosystems," *Optics* **2**(4), 47–50 (2013).
10. M. Hybertsen and S. Louie, "Ab initio static dielectric matrices from the density-functional approach. I. Formulation and application to semiconductors and insulators," *Phys. Rev. B* **35**(11), 5585–5601 (1987).
11. Ab initio calculation, http://sites.google.com/a/kdpu.edu.ua/calculationphysics (2015).
12. R. M. Balabai and H. N. Chernikova, "Platinum-nickel alloy catalysts for fuel elements," *Appl. Phys. A* **116**(2), 649–655 (2014).
13. R. M. Balabai et al., "Electron structure and dielectric matrix of the model photonic crystals formed by fibers: ab initio calculation," *Nanosyst. Nanomater. Nanotechnol.* **13**(4), 707–720 (2015).
14. R. M. Balabai, D. Gritsulia, and V. G. Litovchenko, "Tuning of electron states of transition metal's catalysts using acceptor's atoms: ab initio calculation," *J. Nano-Electron. Phys.* **8**(2), 02007 (2016).
15. R. M. Balabai and D. Kravtsova, "Anomalous electronic properties of thin metal films of island structures: the first principles calculations," *J. Phys. Stud.* **21**(1/2), 1703 (2017).
16. R. M. Balabai and D. Kravtsova, "Hardness of diamond-cBN nanocomposite," *Diamond Relat. Mater.* **82**, 56–62 (2018).
17. P. Hohenberg and W. Kohn, "Inhomogeneous electron gas," *Phys. Rev.* **136**(3B), B864 (1964).
18. W. Kohn and L. Sham, "Self-consistent equations including exchange and correlation effects," *Phys. Rev.* **140**(4A), A1133 (1965).
19. G. Bachelet, D. Hamann, and M. Schlüter, "Pseudopotentials that work: from H to Pu," *Phys. Rev. B* **26**(8), 4199–4228 (1982).
20. J. Ihm, A. Zunger, and M. Cohen, "Momentum-space formalism for the total energy of solids," *J. Phys. C: Solid State Phys.* **12**(21), 4409–4422 (1979).
21. M. Payne et al., "Iterative minimization techniques for ab initio total-energy calculations: molecular dynamics and conjugate gradients," *Rev. Mod. Phys.* **64**(4), 1045–1097 (1992).
22. A. G. Marinopoulos et al., "Ab initio study of the optical absorption and wave-vector-dependent dielectric response of graphite," *Phys. Rev. B* **69**, 245419 (2004).
23. M. Gajdoš et al., "Linear optical properties in the projector-augmented wave methodology," *Phys. Rev. B* **73**, 045112 (2006).

Biographies for the authors are not available.